

Article

Alkali and Alkaline Earth Cation-Decorated TiO₂ Nanotube-Supported Rh Catalysts for Vinyl Acetate Hydroformylation

Hongyuan Chuai ¹ , Penghe Su ¹, Hongchi Liu ¹, Baolin Zhu ^{1,2}, Shoumin Zhang ^{1,2} and Weiping Huang ^{1,2,3,*}

¹ College of Chemistry, Nankai University, Tianjin 300071, China; chuaihongyuan0108@163.com (H.C.); sph_edu@163.com (P.S.); h335liu@edu.uwaterloo.ca (H.L.); zhubaolin@nankai.edu.cn (B.Z.); zhangsm@nankai.edu.cn (S.Z.)

² The Key Laboratory of Advanced Energy Materials Chemistry (Ministry of Education), Nankai University, Tianjin 300071, China

³ Collaborative Innovation Center of Chemical Science and Engineering, Tianjin 300071, China

* Correspondence: hwp914@nankai.edu.cn; Tel.: +86-138-2009-6974

Received: 20 November 2018; Accepted: 13 February 2019; Published: 20 February 2019



Abstract: Alkali and alkaline earth cation-decorated TiO₂ nanotube (TNT)-supported rhodium catalysts were synthesized and characterized by inductively-coupled plasma optical emission spectrometer, surface characterization analyzer, X-ray diffraction, transmission electron microscopy, X-ray photoelectron spectroscopy, and Fourier transforming infrared spectrum, respectively. Their catalytic performances were evaluated by the hydroformylation of vinyl acetate. Results showed that both the conversion rate of vinyl acetate and selectivity for aldehyde were improved after Rh/TNTs were modified by alkali or alkali-earth cations. Such improved selectivity for aldehyde might be attributed to the presence of alkali or alkaline earth cations which enhanced CO adsorption, while the high conversion rate of vinyl acetate was likely due to the proper interaction of Lewis acid–base between cations modified TNTs and vinyl acetate.

Keywords: hydroformylation; vinyl acetate; TiO₂ nanotubes; Rh nanoparticles; cations

1. Introduction

Hydroformylation is a classic reaction to produce aldehydes, alcohols or carboxylic acids which are versatile intermediates and building blocks for pharmaceuticals, commodity and fine chemicals [1–4]. Consequently, researchers have been made much effort to increase the reaction rate of hydroformylation and the selectivity of aldehyde over the past years [5,6]. Up to now, the hydroformylation of functionalized terminal olefin, such as vinyl acetate, is still a charming topic since its functional group may coordinate to the metal center [7,8]. This chelation may cut down the catalytic activity of catalytic center and then have negative effect on the catalyst. In order to weaken this effect, we attempted to design a novel catalysis system with two active center, Rh-Ru/TNTs, in which Ru active center as Lewis acid attracts vinyl acetate through the carboxyl (Lewis base) and accordingly reduces the influence of the carboxyl on Rh active center, leading to improved conversion of vinyl acetate in hydroformylation after introducing Ru into Rh/TNTs [9]. Unfortunately, the chemical selectivity for aldehyde over Rh-Ru/TNTs decreased in comparison with that of Rh/TNTs. We also tried Au-Rh catalysis system by replacing Ru with Au, the results, however, are frustratingly founding that though the chemical selectivity for aldehyde was increased, there was no significant change in the conversion rate [10]. Therefore, it is necessary to develop a new functional catalyst which has better catalytic performance.

In the study of literature, we found that a great deal of literature has reported that alkali and alkaline-earth metals, particularly potassium, are used as promoters to increase the activity of iron-based catalyst for Fischer–Tropsch synthesis (FTS) and water-gas shift (WGS) reaction [11–16]. The causation is normally explained as the electropositivity of the alkali element promoter results in a charge transfer from the alkali promoter to the surface of transition metal, enhancing CO adsorption [17,18]. In the hydroformylation, CO is also the main reactant, and alkali metals in catalysts might show the similar effect. In fact, there are some studies [19,20] that reported that the alkali cations acted as promoters and enhanced the selectivity for aldehyde in the hydroformylation reaction. For instance, in a previous study, the influence of the cationic promoters on rhodium was examined in the hydroformylation of ethene using silica-supported $M_2[Rh_{12}(CO)_{30}]$ ($M = Li, Na, K$) species [19]. Additionally, the influence of the cationic promoters ($M = Li, Na, K, Rb, Cs$) on silica-supported rhodium catalysts was examined in the hydroformylation of propene [20]. However, the application of alkali promoters in hydroformylation of functionalized alkene, e.g., vinyl acetate, is rarely reported.

On the other hand, in order to separate the homogeneous catalysts from the reaction system easily, many inorganic or organic materials are used as supports for Rh-based catalysts. Among these supports, TiO_2 nanotubes (TNTs), which are produced by hydrothermal synthesis, have received increasing attention due to their unique physicochemical properties, such as nanotubular structure with layered walls, high surface area, ion-exchange ability, and photocatalytic activity [21]. In our previous work, we have utilized TNTs as support for Rh-based catalysts and demonstrated that the surface acidity of TNTs may effectively affect the activity of the metal-supported catalysts in hydroformylation of olefins based on the Lewis acid-base model [22,23]. Alkali or alkaline earth cation can not only act as the Lewis acid site, but also enhance CO adsorption according to the literatures on FTS and WGS, if we introduce alkali or alkaline earth cation to decorate the support TNTs, what will happen? In this contribution, we designed alkali and alkaline earth cations modified TNTs supported Rh-nanoparticle catalysts and explored the effects of alkali and alkaline earth cations on the catalytic performances of the catalysts for the hydroformylation of vinyl acetate.

2. Results and Discussion

2.1. Characterization of the Catalysts

All catalysts were prepared by impregnation-reduction procedure. The detailed composition for these catalysts and their surface area (SSA) are given in Table 1. The content of Rh or other metal cations in catalysts was studied by inductively coupled plasma optical emission spectrometer analysis, demonstrating that the presence of alkali or alkaline earth cations did not affect the practical loading of bulk Rh in the catalysts since the nominal Rh loading kept constant or even a bit higher when alkali or alkaline earth cations exist. This result indicates that the addition of alkali or alkaline earth cations little occupied the active sites of TNTs and may be even in favor of Rh loading. Moreover, the Rh content of Rh0.5/Li-TNTs-B1 and Rh0.5/Li-TNTs-B5 is much lower than that of other catalysts with the same nominal Rh loading. It suggests that the reduce method affected on the loading of Rh. The SSA of catalysts was calculated using Brunauer–Emmett–Teller (BET) model. The SSA of Rh0.5/Mg-TNTs-P5 was close to that of Rh0.5/TNTs-P, indicating that the existence of Mg cations does not affect the structure of support. Such observation was further confirmed by X-ray diffraction characterization.

The XRD patterns of pristine TNTs or cations decorated TNTs supported Rh catalysts are shown in Figure 1. All the catalysts display the same diffraction peaks compared to the reported pure TNTs [9]. The assignment of the structure of titanate nanotubular was the subject of intense controversy [24]. In our previous report, the main diffraction peaks of TNTs were assigned as anatase phase of TiO_2 [9,25,26]. However, the samples indeed present four broad diffraction peaks located at 9.58° , 24.36° , 28.36° , and 48.44° which can be attributed to the (020), (110), (130), and (200) crystal planes of orthorhombic lepidocrocite-type titanate on the basis of literature [27–29]. Except the main peaks for the TNTs support, there is no any diffraction peaks related to Rh nanoparticles or other salts in

all samples. This indicates that Rh nanoparticles or other salts in the as-prepared catalysts might be well dispersed on the support and the content of Rh nanoparticles or other salts might be too low to be detected by XRD technique [26].

TEM analysis was subsequently adapted to observe the morphology of catalysts and identify the existence of Rh nanoparticles (Figure 2). All catalysts display perfect tubular multiwall structure, which further manifests that the introduction of alkali or alkaline earth cations has no apparent effect on the morphology of TNTs (Figure 2A–F). The interlayer spacing of prepared TNTs is about 0.7 nm and the diameter of TNTs or cation-modified TNTs is about 10 nm [22] (Figure 2A–F). As for the catalyst Rh0.5/Li-TNTs-B5 prepared by borohydride-reduction (Figure 2B), we can see obvious Rh nanoparticles anchored to the surface or the interspace of the supporter of Li-TNTs. The size distribution of Rh nanoparticles was statistically calculated and exhibited in Supplementary Materials Figure S1. The average size of Rh nanoparticles is about 1.27 nm. However, only some black spots can be seen on the Rh0.5/Li-TNTs-P5 catalyst (Figure 2A) or other alkaline earth cation-contained catalysts (Figure 2C–F). This illustrates that the procedure of reduction affects the size of Rh particles in the catalyst, and the much stronger reducibility of borohydride may result in the formation of larger Rh particles, which has been elucidated intensively in our previous report [26]. It is worth noting that though the size of Rh nanoparticles in catalyst Rh0.5/Li-TNTs-B5 are much bigger than that in the other catalysts, they also don't show any diffraction peaks in the XRD spectra probably due to the low concentration and high dispersion of Rh nanoparticles [10]. Apart from the observation above, it was found that there are no significant difference in morphology for the fresh and used Rh0.5/Sr-TNTs-P5 catalyst (Figure 2E,F), demonstrating that M-TNTs are quite stable keeping perfect in the process of hydrformylation.

Table 1. The preparation method, the content of Rh or M (M = Li, Na, K, Mg, Ca, Sr.) promoters, and the specific surface area (SSA) of catalysts.

Entry	Catalyst	Rh (Nominal) (wt.%)	M/Rh (Nominal) (Molar Ratio)	Reduction Method	Rh, M ICP (wt.%)	SSA BET (m ² /g)
1	Rh0.5/TNTs-P	0.5	—	photo-reduction	0.35, —	300.08
2	Rh0.25/TNTs-P	0.25	—	photo-reduction	0.20, —	—
3	Rh0.1/TNTs-P	0.1	—	photo-reduction	0.15, —	302.83
4	Rh0.5/Li-TNTs-P1	0.5	1	photo-reduction	0.43, 0.02	—
5	Rh0.5/Li-TNTs-P5	0.5	5	photo-reduction	0.38, 0.08	—
6	Rh0.5/Li-TNTs-B1	0.5	1	borohydride	0.27, 0.04	—
7	Rh0.5/Li-TNTs-B5	0.5	5	borohydride	0.27, 0.10	—
8	Rh0.25/Li-TNTs-P5	0.25	5	photo-reduction	0.26, 0.07	—
9	Rh0.1/Li-TNTs-P5	0.1	5	photo-reduction	0.15, 0.04	—
10	Rh0.5/Na-TNTs-P5	0.5	5	photo-reduction	0.38, 3.45	—
11	Rh0.5/K-TNTs-P5	0.5	5	photo-reduction	0.38, 1.01	—
12	Rh0.5/Mg-TNTs-P5	0.5	5	photo-reduction	0.37, 0.57	301.49
13	Rh0.1/Mg-TNTs-P5	0.1	5	photo-reduction	0.17, 0.22	—
14	Rh0.5/Ca-TNTs-P5	0.5	5	photo-reduction	0.36, 0.95	—
15	Rh0.1/Ca-TNTs-P5	0.1	5	photo-reduction	0.14, 0.30	—
16	Rh0.5/Sr-TNTs-P5	0.5	5	photo-reduction	0.40, 1.29	—
17	Rh0.1/Sr-TNTs-P5	0.1	5	photo-reduction	0.12, 0.50	—

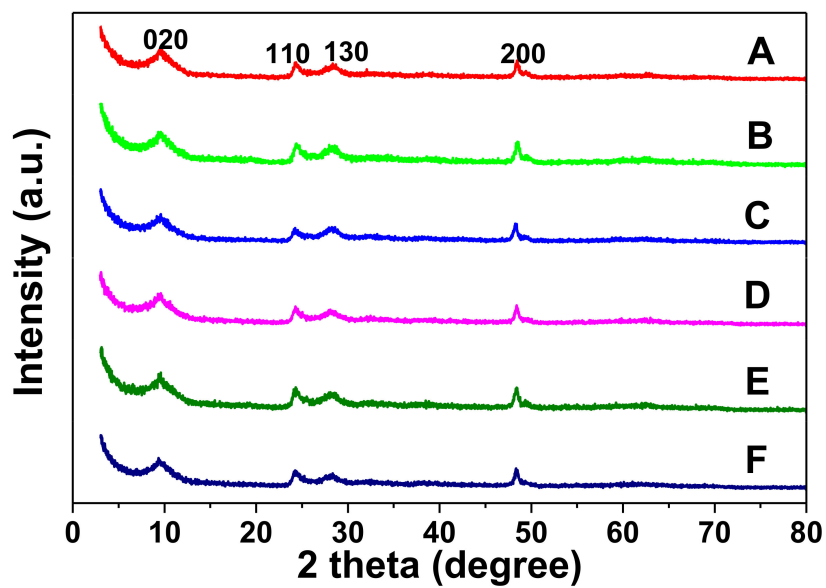


Figure 1. XRD patterns of samples: Rh0.5/TNTs-P (A), Rh0.5/Li-TNTs-P5 (B), Rh0.5/Li-TNTs-B5 (C), Rh0.5/Mg-TNTs-P5 (D), Rh0.5/Ca-TNTs-P5 (E), and Rh0.5/Sr-TNTs-P5 (F).

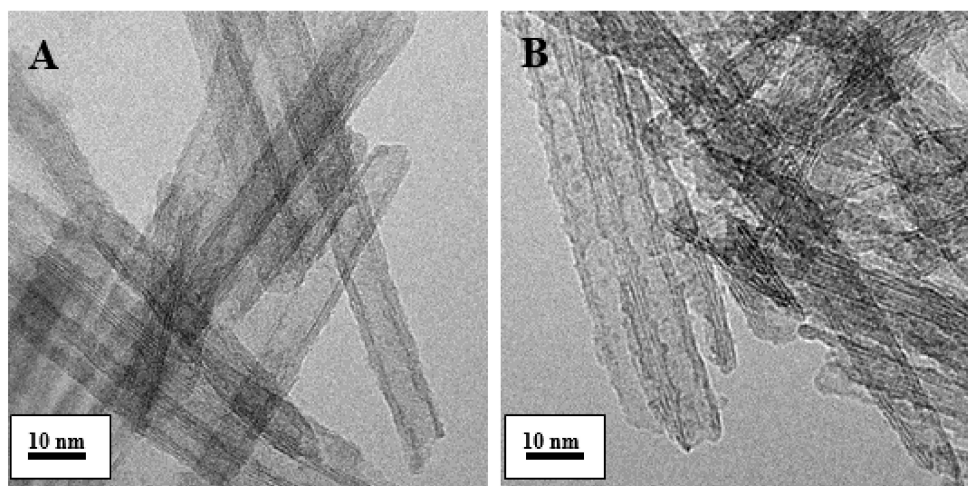


Figure 2. *Cont.*

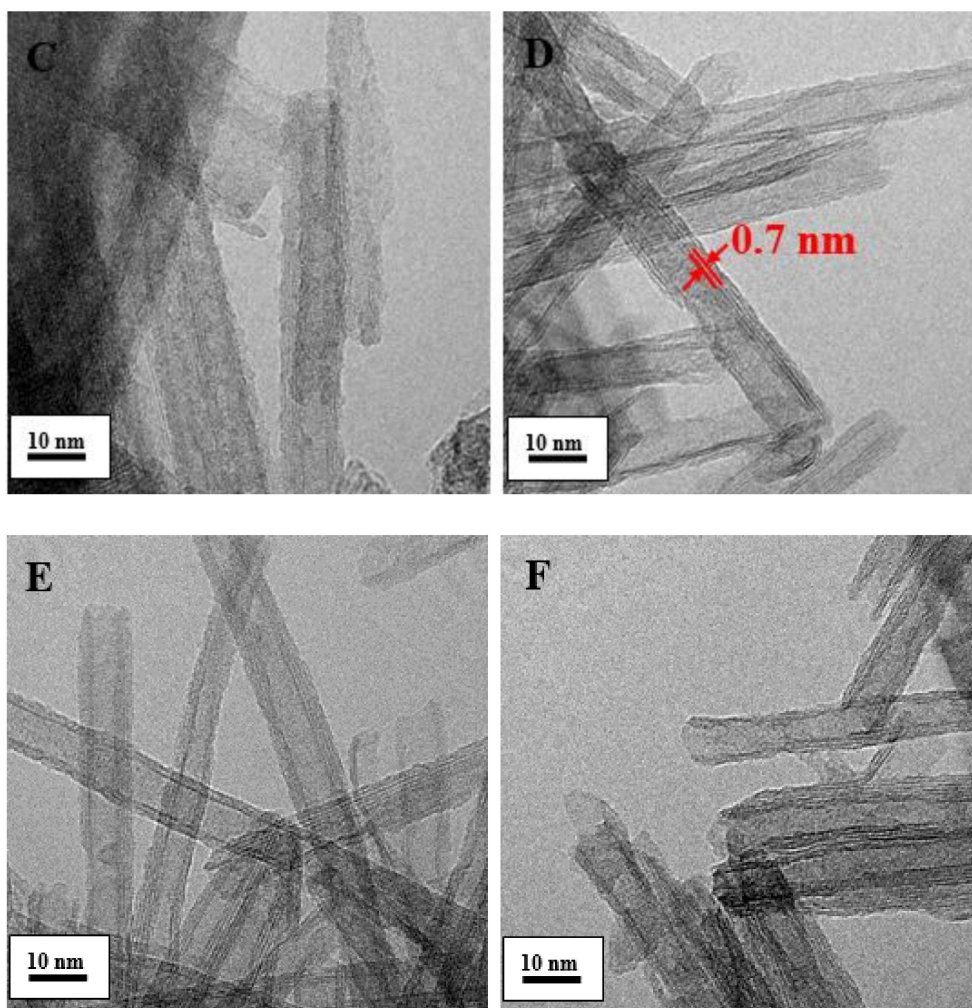


Figure 2. The TEM images of samples: Rh_{0.5}/Li-TNTs-P5 (A), Rh_{0.5}/Li-TNTs-B5 (B), Rh_{0.5}/Mg-TNTs-P5 (C), Rh_{0.5}/Ca-TNTs-P5 (D), Rh_{0.5}/Sr-TNTs-P5 fresh (E), and used (F).

In order to learn about the chemical state of Rh nanoparticles and to explore the interaction among Rh nanoparticles, TNTs supporter and cations, we selected pure Rh catalyst and Li- or Mg-containing catalyst as examples and characterized them with X-ray photoelectron spectroscopy. As shown in Figure 3, Rh nanoparticles in all samples exist as two chemical states Rh⁰ and Rh²⁺, in which Rh 3d 5/2 and Rh²⁺ 3d 5/2 peaks located at about 306.7 eV and 308.0 eV, respectively [10,30]. The oxide species Rh²⁺ might be caused by the samples being exposed to air during collection and waiting for characterization. The cations, such as Mg species, they exist as Mg²⁺ ions in Rh_{0.5}/Mg-TNTs-P5 catalyst according to the XPS spectra shown in Supplementary Materials Figure S2 [31] and they may be adsorbed on the TNTs. As literature reported, the multi-layered nanotube TNTs were constructed by rolling up one [1 0 1] layer of the anatase structure along the [−1 0 1] direction and there are a lot of unsaturated oxygen atom which can be the active site for Rh²⁺ ions and promoter Mg²⁺ ions [32,33].

Compared with pure TNTs supported Rh catalyst, we can find that the binding energy of Rh 3d in Li or Mg-contained catalyst keeps the same value as pure TNTs catalyst. It suggests that the chemical environment surrounding the Rh nanoparticles have no significant change with modifying TNTs support. However, the binding energy of Rh²⁺ 3d in Li or Mg-contained catalyst shifts to a higher value, especially Mg-containing catalyst, indicating that the electronic density of Rh²⁺ species decreased [34,35]. Besides, from the area of the fitted Gauss peaks, it is easy to find that Rh⁰ is the major Rh species for all catalysts. However, the proportion of Rh⁰ in Mg-contained catalyst is much

higher than that in Rh0.5/TNTs-P and Rh0.5/Li-TNTs-P5, indicating that Mg^{2+} cations might suppress oxidation of Rh nanoparticles.

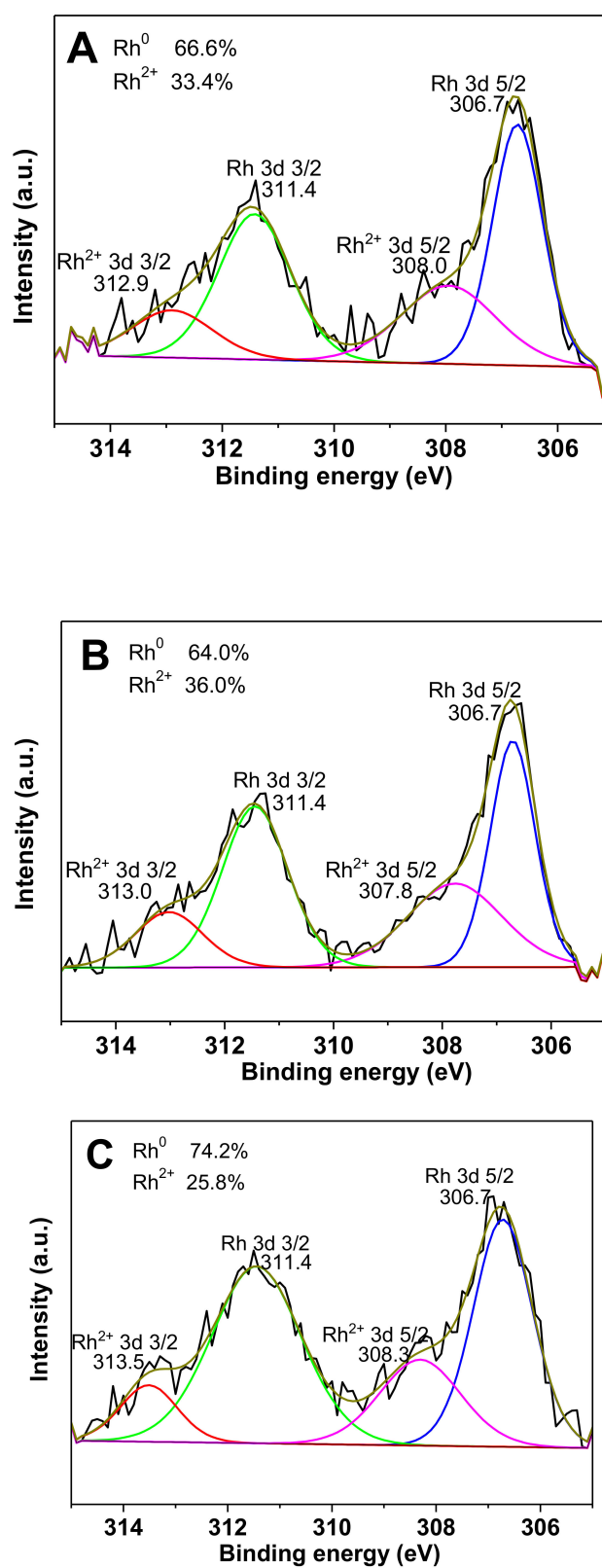


Figure 3. High-resolution XPS spectra of Rh3d in catalysts: Rh0.5/TNTs-P (A), Rh0.5/Li-TNTs-P5 (B), and Rh0.5/Mg-TNTs-P5 (C).

It is well known that CO is an important reactant in the hydroformylation. Herein, we use FT-IR to analyze the CO species adsorbed on catalysts. As we can see from Figure 4, all the samples present the peaks located at 1449 cm^{-1} , 1549 cm^{-1} , and 1630 cm^{-1} , respectively, which can be attributed to the bending vibration of O-H bonds that came from the H_2O molecules adsorbed on surface of the TNTs support [36]. Except the peaks of water molecules, there are no other peak in the spectra of pure TNTs (Figure 4A,B). However, pure TNTs supported Rh catalysts and cationic-contained catalysts display CO absorption peak located around 2068 cm^{-1} , which can be attributed to typical terminal CO adsorbed on the metals (M-CO) [37]. Additionally, the band intensity of carbonyl vibration shows significantly difference among these catalysts. Compared with pure TNTs supported Rh catalysts (Figure 4C,D), the intensity and position of CO peak in Li-contained catalyst increases a little (Figure 4E), while Mg-containing catalyst enhances remarkably (Figure 4F), so as those of Ca and Sr-containing catalysts (Figure 4G,H). This result implies that the introduction of alkali or alkaline earth cations, especially alkaline earth cations, can enhance CO adsorption ability. It can be explained by the interaction between these cations and Rh nanoparticles. CO, a π -acid ligand, tends to be absorbed on Rh nanoparticles which can provide feedback electrons and the electrons may transfer from the d-orbital of Rh to the anti-bonding CO molecular orbital. During this procedure, the charge transferring from alkali or alkaline earth promoter to the surface of Rh metal makes the formation of electrons donated more easily, especially when they carry with high charge, as the alkaline earth promoters. Moreover, the high proportion of Rh^0 in Mg-containing catalyst is also a possible reason based on XPS results.

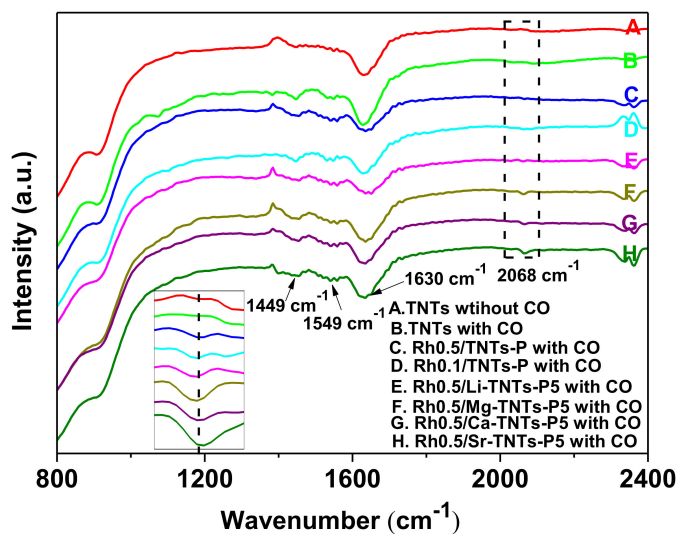
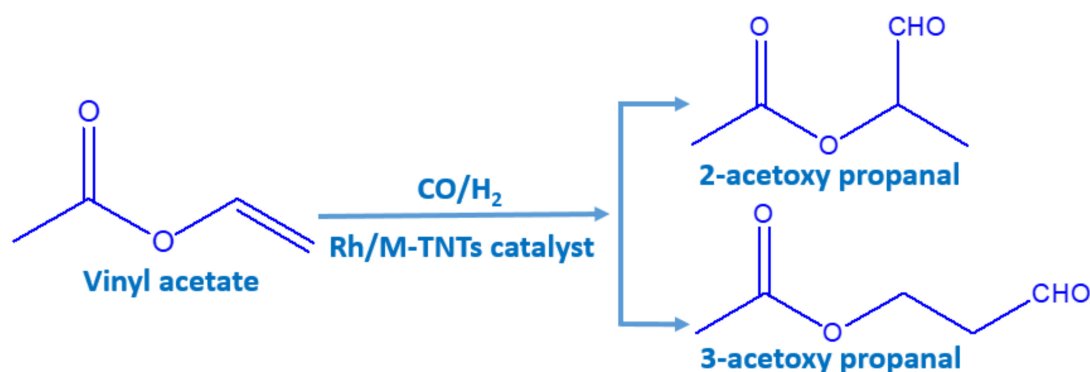


Figure 4. The FT-IR spectra of samples: TNTs without CO gas (A); TNTs with CO gas (B); Rh0.5/TNTs-P with CO gas (C), Rh0.1/TNTs-P with CO gas (D), Rh0.5/Li-TNTs-P5 with CO gas (E), Rh0.5/Mg-TNTs-P5 with CO gas (F), Rh0.5/Ca-TNTs-P5 with CO gas (G), and Rh0.5/Sr-TNTs-P5 with CO gas (H). Inset: expanded view between 2040 and 2090 cm^{-1} .

2.2. Catalytic Performances of the Catalysts

To evaluate the catalytic performance of the catalysts, we carried out experiment on hydroformylation of vinyl acetate. In general, the hydroformylation of vinyl acetate can produce two functional products (Scheme 1). In our experiments, the hydroformylation of vinyl acetate over all catalysts has high regioselectivity for 2-acetoxy propanal (2-acetoxy propanal:3-acetoxy propanal = 100:0) and generates at least other three by-products, ethylene, propanal, and acetic acid. The gas chromatogram of products formed in the hydroformylation of vinyl acetate are shown in Supplementary Materials Figure S3.



Scheme 1. Illustration for vinyl acetate hydroformylation.

In order to explore the effect of alkali or alkaline earth cations on the reaction, we evaluated the catalytic activity of Rh/TNTs with different Rh loadings firstly. Taking into account the effect of actual Rh loading on catalyst activity on the reaction, we calculated an apparent turnover frequency (TOF) of vinyl acetate consumption over all the catalysts. As shown in Table 2, the catalytic activity of Rh/TNTs varies with Rh loading (Entry 1–3). It is obvious that TOF increases with the decrease of Rh loading, and so do the selectivity for aldehyde. This means that there should be an optimal Rh loading; when the Rh loading is larger than the optimal one, the superfluous Rh may not increase the amount of catalytic active site efficiently. As for the reason that the selectivity for aldehyde increases as Rh loading decreases, it could be deduced by the good distribution of Rh nanoparticles on the surface of TNTs for the low Rh loading catalyst which benefits the interaction among Rh nanoparticles, TNTs and substrate. Compared to Rh/TNTs, all the alkali or alkaline earth cations modified TNTs supported Rh catalyst show better catalytic activity, both in the conversion of vinyl acetate and the selectivity for aldehyde. Furthermore, the impact level of alkali and alkaline earth cations on the catalytic performance has to do with the preparation method of catalysts, Rh loading and the species of cations. For instance, the catalytic activity of Li-contained catalyst prepared by photoreduction is much higher than that by borohydride reduction (Entry 4–7). The reasonable explanation might be that the actual Rh loading is higher and the size of Rh nanoparticles is smaller in the catalyst prepared by photoreduction (Table 1, Figure 2A,B). Comparing Entry 4 with Entry 5, Rh_{0.5}/Li-TNTs-P5 has higher selectivity for aldehyde, and the effect of Li⁺ ions become more remarkable with the increase of the molar ratio of Li to Rh. The optimal molar ratio of Li to Rh should be 5:1.

For Rh/Li-TNTs catalysts, the influence of Li⁺ varies on the catalytic properties with Rh loading. When Rh nominal loading is 0.5%, the selectivity for aldehyde in hydroformylation of vinyl acetate over Rh_{0.5}/Li-TNTs-P5 (Entry 5) is much higher than that over Rh_{0.5}/TNTs-P (Entry 1); when Rh nominal loading is 0.25%, both the conversion of vinyl acetate and the selectivity for aldehyde over Rh_{0.25}/Li-TNTs-P5 (Entry 8) are much higher than those over Rh_{0.25}/TNTs-P (Entry 2); when Rh nominal loading is 0.1%, the conversion of vinyl acetate over Rh_{0.1}/Li-TNTs-P5 (Entry 9) is higher than that over Rh_{0.1}/TNTs-P (Entry 3), but the selectivity for aldehyde is a bit lower. Overall, Rh in Rh_{0.25}/Li-TNTs-P5 shows highest efficient, and the TOF over Rh_{0.25}/Li-TNTs-P5 (Entry 8, the TOF is 3581 h⁻¹) is much higher than that over Rh_{0.25}/TNTs-P (Entry 2, the TOF is 2501 h⁻¹). For Na⁺ and K⁺ containing catalysts, as Rh nominal loading is 0.5%, the selectivity for aldehyde is improved by alkali metal cations and the effect of cation promotor is in the following order: Li⁺ (Entry 5) > Na⁺ (Entry 10) > K⁺ (Entry 11). This result is in accord with literature reports and can be explained by the polarizing power of alkali cations [20]. The higher the polarizing effect of the cation, the stronger interaction among alkali cations, TNTs and Rh nanoparticles. As a result of this interplay, the CO adsorption enhances, the rate of CO insertion improves and then the selectivity for aldehyde increases.

Table 2. Activity and selectivity of all catalysts catalyzed vinyl acetate hydroformylation.

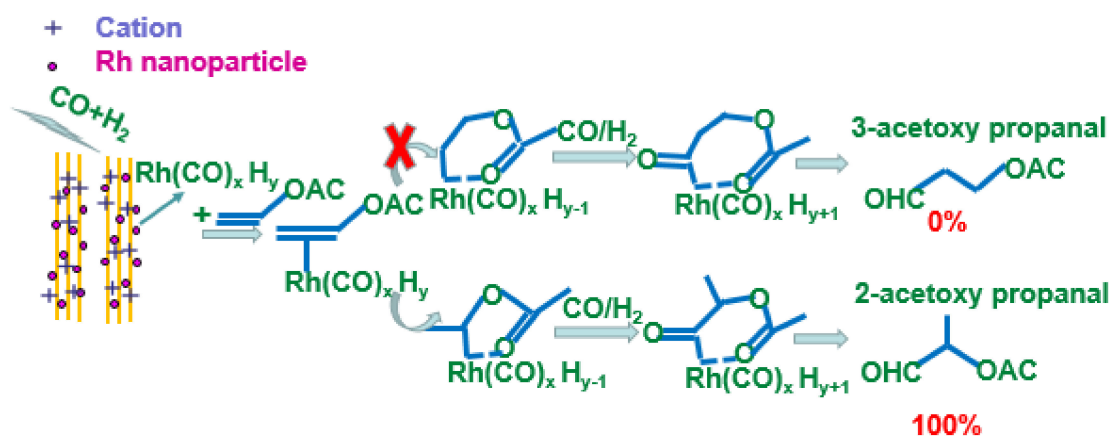
Entry	Catalyst	Conversion of Vinyl Acetate (%)	Selectivity of Aldehyde (%)	TOF ^a (h ⁻¹)
1	Rh0.5/TNTs-P	100	60	2382
2	Rh0.25/TNTs-P	60	60	2501
3	Rh0.1/TNTs-P	40	78	2890
4	Rh0.5/Li-TNTs-P1	100	75	2424
5	Rh0.5/Li-TNTs-P5	100	81	2962
6	Rh0.5/Li-TNTs-B1	70	92	3315
7	Rh0.5/Li-TNTs-B5	84	63	2724
8	Rh0.25/Li-TNTs-P5	100	67	3581
9	Rh0.1/Li-TNTs-P5	44	74	3016
10	Rh0.5/Na-TNTs-P5	100	80	2926
11	Rh0.5/K-TNTs-P5	100	79	2889
12	Rh0.5/Mg-TNTs-P5	99	76	2826
13	Rh0.1/Mg-TNTs-P5	58	64	3034
14	Rh0.5/Ca-TNTs-P5	100	60	2316
15	Rh0.1/Ca-TNTs-P5	46	72	3287
16	Rh0.5/Sr-TNTs-P5	100	77	2675
17	Rh0.1/Sr-TNTs-P5	43	68	3386

Reaction conditions: vinyl acetate = 5 mL, catalyst = 0.40 g, CO/H₂ = 1, solvent (toluene) = 65 mL, and reaction time = 1 h. ^a TOF = number of moles of product formed/(number of moles of Rh × h).

As for catalysts containing alkaline earth cations Mg²⁺, Ca²⁺ and Sr²⁺, the catalytic performance is much better than that pure TNTs supported Rh catalysts, but the effect of alkaline earth cations is not as regularly as alkali cations. This might have to do with the actual Rh loading (Table 1). It is worth noting that when Rh nominal loading is 0.5%, the conversion of vinyl acetate over all of catalysts can reach up to 100%, while the selectivity for aldehyde over Rh0.5/M-TNTs-P5 is much higher than that over Rh0.5/TNTs-P except Rh0.5/Ca-TNTs-P5. Compared with our previous work on Au-Rh/TNTs catalysis system, the conversion of vinyl acetate over cations-containing catalysts improves noticeably though Au could provide free coordination sites for substrates and work synergistically with Rh nanoparticles to enhance the catalytic performance of Rh catalysts [10]. When Rh nominal loading is 0.1%, the conversion of vinyl acetate over Rh0.1/M-TNTs-P5 (M = Li, Mg, Ca, Sr) is higher than that over Rh0.1/TNTs-P while the selectivity for aldehyde is a bit lower. Even so, the selectivity for aldehyde over Rh0.1/M-TNTs-P5 is much higher than that over Rh-Ru/TNTs catalysis system [9]. This might be because that alkali or alkaline earth cations are not a catalyst for hydroformylation or hydrogenation while Ru is a catalyst for hydrogenation [38], as a result, Rh-Ru catalysis system enhance the conversion of vinyl acetate at the meantime strengthen the hydrogenation activity.

On the basis of characterization and experiment results, we propose the possible pathways of the reaction which is shown in Scheme 2. At first, Rh nanoparticles anchored on M-TNTs turn into Rh(CO)_xHy/M-TNTs after bumping the syngas CO and H₂. Then the substrate vinyl acetate coordinate with the catalyst, and the intermediate are formed. In this step, the introduction of cations plays an important role. As we mentioned in the introduction, the acidity of the support has an influence on the activity of Rh catalysts for hydroformylation of olefins. In Rh/M-TNTs catalysis system, cations can be as an electron-deficient center (Lewis acid site) and the carboxyl in vinyl acetate with π bonds tends to be an electron donor (Lewis base) [39,40]. Consequently, vinyl acetate is easily to be adsorbed on the Lewis acid sites with the formation of electron-deficient intermediates and this will help to hydroformylate by CO and H₂. As we proposed in Scheme 2, there can be two kinds of intermediates which are supposed to form the final product 2-acetoxy propanal and 3-acetoxy propanal. However, there is no 3-acetoxy propanal formed. This is because the intermediate with a five-membered ring is more stable [41]. During the CO insertion step, the CO adsorption capacity of the catalyst plays a role. The presence of cations (in particular, alkali earth cations) enhances CO adsorption. This might lead to the higher selectivity for aldehyde. During the process of

hydroformylation, the interplay accompanied by the existence of cations works synergistically and facilitates the reaction effectively.



Scheme 2. Proposed pathways of vinyl acetate hydroformylation over Rh/M—TNTs.

3. Experimental Section

Preparation of modified TNTs support. TNTs were synthesized by the hydrothermal treatment according to the relevant reference [42]. All metal chlorides MCl (M = Li, Na, K, etc.) were analytic reagents and used as such without any further purification. The alkali and alkaline earth cations modified TNTs support (labelled as M-TNTs) was prepared via a simple impregnation procedure. 1.0 g TNTs were dispersed in 10 mL of desired amount salt aqueous solution, and the mixture was agitated for 5 h at 70 °C, then irradiated by ultrasound for 1 h. The solid obtained was dried at 80 °C and grinded to powder.

Preparation of Rh/TNTs catalysts. The synthesis procedure of Rh/TNTs (Rh nominal loading is 0.5%) is described as follows: 1.0 g TNTs were dispersed in 10 mL of aqueous RhCl_3 solution (0.0128 g $\text{RhCl}_3 \cdot 3\text{H}_2\text{O}$), and the mixture was agitated for 5 h at 70 °C, sonicated for 1 h, and then centrifuged. Wash the deposit obtained with a little distilled water, and then transfer it into a 60-mL quartz reactor of 50 mL ethanol-water solution ($V_{\text{ethanol}}:V_{\text{water}} = 9:1$). Then the mixture was irradiated for 4 h with a 300 W high-pressure mercury lamp under stirring at ambient temperature. After that, the mixture was centrifuged and the gray deposit washed with distilled water and ethanol, then dried at 37 °C in vacuum. The finally product obtained was labelled as Rh0.5/TNTs-P.

Preparation of Rh/M-TNTs catalysts. Catalysts, the molar ratio of M/Rh is 5, (nM/nRh = 5, M = Na, K, Mg, Ca, Sr), were prepared by the same impregnation-photoreduction process of preparing Rh/TNTs except that pure TNTs was replaced by M-TNTs and labelled as Rh/M-TNTs-P5. For Rh/Li-TNTs catalyst, we explored different methods of reduction and Li/Rh molar ratios.

Rh0.5/Li-TNTs-P1 (nLi/nRh = 1): prepared by the same impregnation-photoreduction process of preparing Rh/TNTs except that pure TNTs was replaced by Li-TNTs.

Rh0.5/Li-TNTs-P5 (nLi/nRh = 5): prepared by the same impregnation-photoreduction process of preparing Rh/TNTs except that pure TNTs was replaced by Li-TNTs.

Rh0.5/Li-TNTs-B1 (nLi/nRh = 1): prepared by impregnation-borohydride reduction and details are as follows: the impregnation procedure was the same as above. After impregnation, the mixture was transferred into a flask (100 mL) of 20 mL distilled water and the flask was submerged in an ice-water bath. Then excess KBH_4 aqueous solution was added to the flask dropwise while vigorously stirring. After addition of KBH_4 aqueous solution, the mixture was stirred for another 1 h at 0 °C and room temperature, respectively. Then the mixture was centrifuged and the gray product washed to neutral with distilled water and ethanol, then dried at 37 °C in vacuum.

Rh0.5/Li-TNTs-B5 (nLi/nRh = 5): prepared by the impregnation-borohydride reduction mentioned above.

Inductively-Coupled plasma optical emission spectrometry (ICP-OES SpectroBlue, Ametek, Germany) was used to measure Rh or other metal loading in the catalysts. The specific surface area (SSA) of samples was determined by a Micromeritics 3-Flex surface characterization analyzer and calculated using Brunauer-Emmett-Teller (BET) model. X-ray diffraction (XRD, Rigaku D/Max-2500 X-ray diffractometer with Cu K α radiation, Japan) was performed to characterize the phase structure of catalysts and transmission electron microscopy (TEM, 200kV, JEM-2100, Japan) was used to observe the morphology and microstructure of catalysts. The chemical states of Rh and interaction between Rh and other cations in catalysts were evaluated by X-ray photoelectron spectroscopy (XPS) using an Al or Mg X-ray source (Kratos Axis Ultra DLD), and all binding energies (BE) were calibrated using C 1s ($E_b = 284.6$ eV) as reference. FT-IR spectra (USA, Bio-rad, FTS6000) were recorded in the spectral range 0–4000 cm^{-1} (the samples were prepared as KBr wafers, and the weight percentage of the sample in KBr was about 0.5%). All samples were treated in a 250-mL stainless steel autoclave reactor pressurized with CO (1.5 Mpa) for 12 h before testing.

The hydroformylation of vinyl acetate was carried out in a 250-mL stainless steel autoclave reactor with magnetic stirrer. The reactor was charged with required amount of catalyst, substrate and solvent. Prior to reaction, the reactor was sealed and purged with CO or H $_2$ for several times to eliminate air, and then pressurized to a desired pressure with the mixture of CO and H $_2$ ($n_{\text{CO}}/n_{\text{H}_2} = 1$) while stirring. Then the reactor was heated up to the reaction temperature and kept at the same temperature for a fixed time under stirring to meet the demand of the activity tests. After desired reaction time, stop heating and release the gas gradually when the reactor was cooled down to room temperature. Take out of the mixture of reaction, centrifuge and analyze the composition of the mixture by GC analysis (Shimadzu GC-2014 gas chromatograph equipped with a 30 m \times 0.53 mm \times 1.0 μm SE-30 capillary column and a FID).

4. Conclusions

In summary, the present study revealed that Rh nanoparticles, supporter, and cations are the important factors for developing new catalysts for hydroformylation. The presence of alkali and alkaline earth cations in TNT-supported Rh catalysts can effectively enhance the adsorption of CO and the promoting effect of these cations for hydroformylation of vinyl acetate is very inspiring. The TOF of catalyst Rh0.25/Li-TNTs-P5 reached up to 3581 h^{-1} , which is much higher than that of Rh0.25/TNTs-P catalyst (2501 h^{-1}). Other cations also have a positive effect on the reaction to a certain extent. The good catalytic performance gives alkali and alkaline earth cation-modified TNT-supported Rh catalyst systems great potential in industrial applications.

Supplementary Materials: The following are available online at <http://www.mdpi.com/2073-4344/9/2/194/s1>, Figure S1: Size distributions of Rh nanoparticles in catalyst Rh0.5/Li-TNTs-B5 (10 particles selected from Figure 2B and measured by nanomeasure software), Figure S2: XPS spectra of Mg1s in catalyst Rh0.5/Mg-TNTs-P5, Figure S3: Gas chromatogram of vinyl acetate hydroformylation after reaction.

Author Contributions: Conceptualization: H.C.; Data curation: H.C.; Formal analysis: H.C.; Funding acquisition: W.H.; Investigation: H.C.; Methodology: H.C.; Project administration: W.H.; resources: W.H.; Software: H.C.; Supervision: W.H.; Validation: B.Z., S.Z., and W.H.; Visualization: P.S. and H.L.; Writing—original draft: H.C.; Writing—review and editing: H.C.

Funding: This research was funded by [National Natural Science Foundation of China] grant number 21373120 and 21071086; [111 Project] grant number B12015.

Conflicts of Interest: The authors declare no conflict of interest.

References

1. Goanvic, L.L.; Ternel, J.; Couturier, J.L.; Dubois, J.L.; Carpentier, J.F. Rhodium-biphephos-catalyzed tandem isomerization–hydroformylation of oleonitrile. *Catalysts* **2018**, *8*, 21. [[CrossRef](#)]
2. Cousin, K.; Menuel, S.; Monflier, E.; Hapiot, F. Hydroformylation of alkenes in a planetary ball mill: From additive-controlled reactivity to supramolecular control of regioselectivity. *Angew. Chem. Int. Ed.* **2017**, *56*, 10564–10568. [[CrossRef](#)] [[PubMed](#)]
3. Ma, Y.B.; Fu, J.; Gao, Z.X.; Zhang, L.B.; Li, C.Y.; Wang, T.F. Dicyclopentadiene hydroformylation to value-added fine chemicals over magnetically separable Fe₃O₄-supported Co-Rh bimetallic catalysts: Effects of cobalt loading. *Catalysts* **2017**, *7*, 103. [[CrossRef](#)]
4. Wang, Y.Q.; Yan, L.; Li, C.Y.; Jiang, M.; Wang, W.L.; Ding, Y.J. Highly efficient porous organic copolymer supported Rh catalysts for heterogeneous hydroformylation of butenes. *Appl. Catal. A Gen.* **2018**, *551*, 98–105. [[CrossRef](#)]
5. Kontkanen, M.J.; Tuikka, M.; Kinnunen, N.M.; Suvanto, S.; Haukka, M. Hydroformylation of 1-hexene over Rh/nano-oxide catalysts. *Catalysts* **2013**, *3*, 324–337. [[CrossRef](#)]
6. Zhao, Y.P.; Zhang, X.M.; Sanjeevi, J.; Yang, Q.H. Hydroformylation of 1-octene in Pickering emulsion constructed by amphiphilic mesoporous silica nanoparticles. *J. Catal.* **2016**, *334*, 52–59. [[CrossRef](#)]
7. Gual, A.; Godard, C.; Castillon, S.; Claver, C. Highly efficient Rhodium catalysts for the asymmetric hydroformylation of vinyl and allyl ethers using C1-symmetrical diphosphite ligands. *Adv. Synth. Catal.* **2010**, *352*, 463–477. [[CrossRef](#)]
8. Khan, S.R.; Bhanage, B.M. Regioselective hydroformylation of vinyl esters catalyzed by Rh(acac)(CO)₂ with simple and efficient diphosphinite ligands. *Catal. Commun.* **2014**, *46*, 109–112. [[CrossRef](#)]
9. Chuai, H.Y.; Liu, X.T.; Chen, Y.; Zhu, B.L.; Zhang, S.M.; Huang, W.P. Hydroformylation of vinyl acetate and cyclohexene over TiO₂ nanotube supported Rh and Ru nanoparticle catalysts. *RSC Adv.* **2018**, *8*, 12053–12059. [[CrossRef](#)]
10. Chen, Y.; Su, P.H.; Liu, T.; Liu, H.C.; Zhu, B.L.; Zhang, S.M.; Huang, W.P. Titanate nanotube-supported Au–Rh bimetallic catalysts: Characterization and their catalytic performances in hydroformylation of vinyl acetate. *Catalysts* **2018**, *8*, 420. [[CrossRef](#)]
11. Li, J.F.; Cheng, X.F.; Zhang, C.H.; Chang, Q.; Wang, J.; Wang, X.P.; Lv, Z.G.; Dong, W.S.; Yang, Y.; Li, Y.W. Effect of alkalis on iron-based Fischer-Tropsch synthesis catalysts: Alkali-FeOx interaction, reduction, and catalytic performance. *Appl. Catal. A Gen.* **2016**, *528*, 131–141. [[CrossRef](#)]
12. Tao, Z.C.; Yang, Y.; Zhang, C.H.; Li, T.Z.; Wang, J.H.; Wan, H.J.; Xiang, H.W.; Li, Y.W. Effect of calcium promoter on a precipitated iron–manganese catalyst for Fischer–Tropsch synthesis. *Catal. Commun.* **2006**, *7*, 1061–1066. [[CrossRef](#)]
13. Pour, A.N.; Shahri, S.M.K.; Bozorgzadeh, H.R.; Tavasoli, Y.Z.A.; Marvast, M.A. Effect of Mg, La and Ca promoters on the structure and catalytic behavior of iron-based catalysts in Fischer–Tropsch synthesis. *Appl. Catal. A Gen.* **2008**, *348*, 201–208. [[CrossRef](#)]
14. Li, J.F.; Zhang, C.H.; Cheng, X.F.; Qing, M.; Xu, J.; Wu, B.S.; Yang, Y.; Li, Y.W. Effects of alkaline-earth metals on the structure, adsorption and catalytic behavior of iron-based Fischer–Tropsch synthesis catalysts. *Appl. Catal. A Gen.* **2013**, *464–465*, 10–19. [[CrossRef](#)]
15. Farias, F.E.M.; Sales, F.G.; Fernandes, F.A.N. Effect of operating conditions and potassium content on Fischer-Tropsch liquid products produced by potassium-promoted iron catalysts. *J. Nat. Gas Chem.* **2008**, *17*, 175–178. [[CrossRef](#)]
16. Zhao, G.Y.; Zhang, C.H.; Qin, S.D.; Xiang, H.W.; Li, Y.W. Effect of interaction between potassium and structural promoters on Fischer–Tropsch performance in iron-based catalysts. *J. Mol. Catal. A Chem.* **2008**, *285*, 137–142. [[CrossRef](#)]
17. Hussain, S.T.; Nadeem, M.A.; Mazhar, M. Effect of potassium addition on the product selectivity of Ru:Mn/alumina supported catalyst system for Fischer–Tropsch reaction. *Catal. Commun.* **2008**, *9*, 2048–2052. [[CrossRef](#)]
18. Yang, Y.; Xiang, H.W.; Xu, Y.Y.; Bai, L.; Li, Y.W. Effect of potassium promoter on precipitated iron-manganese catalyst for Fischer–Tropsch synthesis. *Appl. Catal. A Gen.* **2004**, *266*, 181–194. [[CrossRef](#)]

19. Fusi, A.; Psaro, R.; Dossi, C.; Garlaschelli, L.; Cozzi, F. A molecular approach to heterogeneous catalysis. Ethylene hydroformylation catalysed by silica-supported $[\text{Rh}_{12}(\text{CO})_{30}]^{2-}$ cluster anion: Influence of the counteranions Li^+ , Na^+ , K^+ , Zn^{2+} . *J. Mol. Catal. A*. **1996**, *107*, 255–261. [[CrossRef](#)]
20. Sordelli, L.; Guidotti, M.; Andreatta, D.; Vlaic, G.; Psaro, R. Characterization and catalytic performances of alkali-metal promoted Rh/SiO₂ catalysts for propene hydroformylation. *J. Mol. Catal. A Chem.* **2003**, *204*, 509–518. [[CrossRef](#)]
21. Liu, N.; Chen, X.Y.; Zhang, J.L.; Schwanka, J.W. A review on TiO₂-based nanotubes synthesized via hydrothermal method: Formation mechanism, structure modification, and photocatalytic applications. *Catal. Today* **2014**, *225*, 34–51. [[CrossRef](#)]
22. Li, J.; Chen, Y.; Jiang, Y.J.; Zhu, B.L.; Zhang, S.M.; Hunag, W.P. Ti-O nanotubes supported Rh-catalysts and their catalytic performances for hydroformylation reaction of olefin containing—CN Functional group. *J. Mol. Catal.* **2016**, *30*, 505–514.
23. Shi, Y.K.; Hu, X.J.; Chen, L.; Lu, Y.; Zhu, B.L.; Zhang, S.M.; Huang, W.P. Boron modified TiO₂ nanotubes supported Rh-nanoparticle catalysts for highly efficient hydroformylation of styrene. *New J. Chem.* **2017**, *14*, 6120–6126. [[CrossRef](#)]
24. Gannouna, C.; Turki, A.; Kochkar, H.; Delaigle, R.; Eloy, P.; Ghorbel, A.; Gaigneaux, E.M. Elaboration and characterization of sulfated and unsulfated V₂O₅/TiO₂ nanotubes catalysts for chlorobenzene total oxidation. *Appl. Catal. B Environ.* **2014**, *147*, 58–64. [[CrossRef](#)]
25. Hu, X.J.; Shi, Y.K.; Zhang, Y.J.; Zhu, B.L.; Zhang, S.M.; Huang, W.P. Nanotubular TiO₂-supported amorphous Co-B catalysts and their catalytic performances for hydroformylation of cyclohexene. *Catal. Commun.* **2015**, *59*, 45–49. [[CrossRef](#)]
26. Shi, Y.K.; Hu, X.J.; Zhu, B.L.; Wang, S.R.; Zhang, S.M.; Huang, W.P. Synthesis and characterization of TiO₂ nanotube supported Rh-nanoparticle catalysts for regioselective hydroformylation of vinyl acetate. *RSC Adv.* **2014**, *4*, 62215–62222. [[CrossRef](#)]
27. Ma, R.; Fukuda, K.; Sasaki, T.; Osada, M.; Bando, Y. Structural features of titanate nanotubes/nanobelts revealed by raman, X-ray absorption fine structure and electron diffraction characterizations. *J. Phys. Chem. B* **2005**, *109*, 6210–6214. [[CrossRef](#)] [[PubMed](#)]
28. Mao, Y.; Wong, S.S. Size- and shape-dependent transformation of nanosized titanate into analogous anatase titania nanostructures. *J. Am. Chem. Soc.* **2006**, *128*, 8217–8226. [[CrossRef](#)] [[PubMed](#)]
29. Liu, P.R.; Zhang, H.M.; Liu, H.W.; Wang, Y.; Yao, X.D.; Zhu, G.S.; Zhang, S.Q.; Zhao, H.J. A facile vapor-phase hydrothermal method for direct growth of titanate nanotubes on a titanium substrate via a distinctive nanosheet roll-up mechanism. *J. Am. Chem. Soc.* **2011**, *133*, 19032–19035. [[CrossRef](#)] [[PubMed](#)]
30. Dennis, A.M.; Howard, R.A.; Kadish, K.M.; Bean, J.L.; Brace, J.; Winograd, N. X-ray photoelectron spectra of some dirhodium carboxylate complexes. *Inorg. Chim. Acta* **1980**, *44*, L139–L141. [[CrossRef](#)]
31. Seyama, H.; Soma, M. X-ray photoelectron spectroscopic study of montmorillonite containing exchangeable divalent cations. *J. Chem. Soc. Faraday Trans.* **1984**, *80*, 237–248. [[CrossRef](#)]
32. Bandura, A.V.; Evarestov, R.A. From anatase (1 0 1) surface to TiO₂ nanotubes: Rolling procedure and first principles LCAO calculations. *Surf. Sci.* **2009**, *603*, L117–L120. [[CrossRef](#)]
33. Hossain, F.M.; Evteev, A.V.; Belova, I.V.; Nowotny, J.; Murch, G.E. Electronic and optical properties of anatase TiO₂ nanotubes. *Comput. Mater. Sci.* **2010**, *48*, 854–858. [[CrossRef](#)]
34. Rasko, J.; Bontovics, J. FTIR study of the rearrangement of adsorbed CO species on Al₂O₃-supported rhodium catalysts. *Catal. Lett.* **1999**, *58*, 27–32. [[CrossRef](#)]
35. Ding, D.; Yu, J.; Guo, Q.S.; Guo, X.M.; Xiao, X.J.; Mao, D.S.; Lu, G.Z. The effects of PVP-modified SiO₂ on the catalytic performance of CO hydrogenation over Rh–Mn–Li/SiO₂ catalysts. *RSC Adv.* **2017**, *7*, 48420–48428. [[CrossRef](#)]
36. Zhang, S.H.; Han, X.X. Study on preparation and morphology of Aluminum-coated titanium dioxide. *Semicond. Optoelectronics* **2018**, *39*, 65–76.
37. Flores-Escamilla, G.A.; Fierro-Gonzalez, J.C. Infrared spectroscopic study of dimethyl ether carbonylation catalysed by TiO₂-supported rhodium carbonyls. *Catal. Sci. Technol.* **2015**, *5*, 843–850. [[CrossRef](#)]
38. Iqbal, S.; Kondrat, S.A.; Jones, D.R.; Schoenmakers, D.C.; Edwards, J.K.; Lu, L.; Yeo, B.R.; Wells, P.P.; Gibson, E.K.; Morgan, D.J.; et al. Ruthenium nanoparticles supported on carbon: An active catalyst for the hydrogenation of lactic acid to 1,2-propanediol. *ACS Catal.* **2015**, *5*, 5047–5059. [[CrossRef](#)]

39. Ichikawa, M.; Lang, A.J.; Shriver, D.F.; Sachtler, W.M.H. Selective hydroformylation of ethylene on rhodium-zinc-silica. An apparent example of site isolation of rhodium and Lewis acid-promoted carbonyl insertion. *J. Am. Chem. Soc.* **1985**, *107*, 7216–7218. [[CrossRef](#)]
40. Sachtler, W.M.H.; Ichikawa, M. Catalytic site requirements for elementary steps in syngas conversion to oxygenates over promoted rhodium. *J. Phys. Chem.* **1986**, *90*, 4752–4758. [[CrossRef](#)]
41. Borole, Y.L.; Chaudhari, R.V. New Route for the Synthesis of Propylene Glycols via Hydroformylation of Vinyl Acetate. *Ind. Eng. Chem. Res.* **2005**, *44*, 9601–9608. [[CrossRef](#)]
42. Suzuki, Y.; Yoshikawa, S. Synthesis and thermal analyses of TiO₂-derived nanotubes prepared by the hydrothermal method. *J. Mater. Res.* **2004**, *19*, 982–985. [[CrossRef](#)]



© 2019 by the authors. Licensee MDPI, Basel, Switzerland. This article is an open access article distributed under the terms and conditions of the Creative Commons Attribution (CC BY) license (<http://creativecommons.org/licenses/by/4.0/>).